Electronic Supplementary Information for

Customizing Topographical Templates for Aperiodic Nanostructures of Block Copolymers *via* Inverse Design

Runrong Zhang, Liangshun Zhang, Jiaping Lin* and Shaoliang Lin*

Shanghai Key Laboratory of Advanced Polymeric Materials, State Key Laboratory of Bioreactor Engineering, Key Laboratory for Ultrafine Materials of Ministry of Education, School of Materials Science and Engineering, East China University of Science and Technology, Shanghai 200237, China

*Corresponding Author E-mail: zhangls@ecust.edu.cn (Zhang L.); jlin@ecust.edu.cn (Lin J.)

Contents

Part A: Computational Model and Inverse Design Algorithm

A.1 Incorporation of constrained fields We consider a system of AB diblock copolymers directed by topographical templates with an array of nanoposts. The system has n monodisperse AB diblock copolymer chains with volume fraction f_A of A-species. The block copolymers are modeled by the Gaussian chains with harmonic stretching energy. In the framework of field-theoretical simulations, the density fields of A and B blocks are characterized by $\rho_A(\mathbf{r})$ and $\rho_B(\mathbf{r})$, respectively. The nanoposts are described by 'cavity' function $h(\mathbf{r})$ varying from 1 at their centers to 0 outside the nanoposts, which is similar to the formula used in the hybrid particle-field simulations.[S1,S2] The decaying of the function is scaled by the radius R_p of nanoposts. For a set of nanoposts, the overall density is written as

$$\rho_P(r) = \sum_{j=1}^{N_P} h(|r - r_j|) = \sum_{j=1}^{N_P} \frac{1}{2}\left[1 - tanh\left((|r - r_j| - R_p)/\delta\right)\right]$$

, where N_p is the number of nanoposts, $\mathbf{r}_j$ is the center of j-th nanopost, and δ characterizes the width of nanopost-polymer interface. The free energy functional F (in units of thermal energy k_BT) for the system is given by

$$F = \frac{1}{V}\int dr \left\{\frac{1}{2}\sum_{I,J\,=\,A,B,P} \chi_{IJ} N \rho_I \rho_J - \sum_{I\,=\,A,B} \omega_I \rho_I + \frac{1}{2}\kappa\left(\sum_{I\,=\,A,B,P} \rho_I - 1\right)^2\right\} - c_B ln\frac{Q}{Vc_B} \qquad \text{(S1)}$$

where $\chi_{IJ}N$ is the combined Flory-Huggins interaction parameter between I- and J-type components. The Helfand-type parameter κ controls the local compressibility of system. c_B and V are the volume fraction of block copolymers and the volume of system, respectively. Q is the single chain partition function. ω_I denotes the chemical potential field of I-type component.

For the inverse design algorithm of topographical templates described in subsection A.2,

the target structures are introduced by constrained fields *via* the Lagrange method.[S3] We suppose that the density ρ_I^T of I-type component is known in certain domains *S*. The constrained functional is given by

$$E_\lambda = \frac{1}{V} \sum_{I=A\ or\ B} \int_S dr \lambda_I \left(\rho_I - \rho_I^T\right) \tag{S2}$$

where λ_I is the Lagrange multiplier of I-type component (*i.e.*, the multiplier λ_I forces the I-type component to form the desired structures in the domains *S*).

Similar to the Fraaije's idea, [S3] a functional is introduced

$$H = F + E_\lambda \tag{S3}$$

Minimization of the functional with respect to the variables ω_I, ρ_I and λ_I yields the equations of self-consistent field theory (SCFT)

$$\frac{\delta H}{\delta \rho_I} = 0 \tag{S4}$$

$$\frac{\delta H}{\delta \omega_I} = 0 \tag{S5}$$

$$\frac{\delta H}{\delta \lambda_I} = 0 \tag{S6}$$

We use the pseudo-spectral method to solve the modified diffusion equations in SCFT. The fields are updated by means of a two-step Anderson mixing scheme. The iteration steps are repeated until the free energy functional *H* reaches a local minimum. For more details on the numerical implementation of SCFT, see the Fredrickson's monograph and our previous works.[S4,S5,S6]

Three types of target structures (constrained fields) are considered in our work, which is shown in Figure S1. Target structure T_1 contains T-junctions and isolated line. T_2 and T_3 are

nested-elbow and large-area aperiodic structures, respectively. To test the validity of our proposed model (the nanoposts are not included), we perform the simulations for the self-assembly of symmetric block copolymers subjected to the constrained fields. For all the simulations, the combined Flory-Huggins parameter is chosen as $\chi_{AB}N$=20. The natural period of self-assembled nanostructures under these conditions is $L_0 \approx 4.0R_g$. In the settings of constrained fields, the density field of A blocks is constrained to $\rho_A^T = 1.0$ (red color), but the remainder of box is free of any constraints (left panels of Figure S1). Right panels of Figure S1 illustrate the final structures of symmetric block copolymers in presence of constrained fields. Since the constrained patterns are not natural morphology, the block copolymers form the lamellae containing predictive defects at specific locations. The observations confirm the fact that our proposed model can reproduce the target structures. It should be pointed out that unlike the straight lamellae in the target structures, the lamellae in the final structures emerge undulations.

A.2 Inverse design algorithm Herein, we present the steps of algorithm to achieve the inverse solutions of topographical templates for given target structures of block copolymers. These steps are illustrated with corresponding results for the target structure T_1, which are shown in Figure 1 of main text. The outline for the inverse design algorithm is listed as follows:

(1st step): The constrained density fields for the target structure are constructed *via* the Lagrange method, which is described in subsection A.1. As a typical example, the density fields for the target structure with T-junctions and isolated line are shown in Figure 1a.

(2nd step): Nanoposts with fixed number N_p and radius R_p are randomly placed into the

nontrivial structure with constrained fields. The nanoposts are assumed to be mobile and preferential to the A blocks (*e.g.*, $\chi_{AP}N$=-20 and $\chi_{BP}N$=20). The hybrid particle-field simulations are performed in this step and more details about the simulations can refer to our previous works.[S2,S7] The procedure is briefly listed: (i) The self-consistent field equations (Eqs. (S4)-(S6)) for the polymer fluids are numerically solved in the real-space. (ii) The motion of nanoposts obeys the Newton's motion equations $r_j^{n+1} = r_j^n + f_j \Delta t + \theta_j$, where r_j^n is the center of *j*-th nanopost at *n*-th iteration and θ_j is the Gaussian white noise. $f_j \equiv -\frac{\partial H}{\partial r_j}$ is the total force acting on the *j*-th nanopost.[S1] It should be mentioned that the A-wetting nanoparticles are migrated into the energetically favorable A-rich domains to depress the contribution of enthalpy.[S8] Furthermore, the nanoparticles are moved to the centers of defects as "fillers", which alleviate the strain energy coming from the conformational entropy of polymer chains.[S9,S10] The inter-particle interaction modeled by repulsive part of Lennard-Jones potential is also included to avoid the overlap of mobile nanoposts. (iii) Step (i) is repeated until the mean-square displacement of nanoposts is less than $10^{-3}R_g^2$ and the condition of $|1-\rho_A-\rho_B-\rho_P| < 10^{-3}$ is satisfied. Such configuration of nanoposts is considered as a candidate solution (Figure 1b).

(3rd step): The same nontrivial structure can be achieved by the self-assembly of block copolymers directed by various arrangements of nanoposts (*i.e.*, degenerate configurations of nanoposts in the topographical templates could produce similar target structure). To account for the fact, n_{degen} independent runs with random initial placement of nanoposts are carried out for each choice of target structure. For the cases of target structures T_1, T_2 and T_3, the values of n_{degen} are set as 200, 200 and 500, respectively. The location of nanoposts and the

free energy of final configuration are recorded. A statistical weight sampling of nanopost locations is calculated by the formula $P(r) = \sum_n g_n(r) e^{-H_n} \Big/ \sum_n e^{-H_n}$, where $g(\mathbf{r})=1$ if nanoposts are located at **r** while $g(\mathbf{r})=0$ if not. H_n denotes the free energy functional of system for the *n*-th run (Eq. (S3)). The probability distribution of nanoposts is plotted in Figure 1c.

(4th step): The value of p_{thresh} is chosen such that the number of deduced nanoposts is close to the input value N_p of nanoposts in the 2nd step. Such arrangement of nanoposts is considered to be an inverse solution, which is illustrated in Figure 1d.

(5th step): A normal forward SCFT simulation is performed for the symmetric block copolymers under the topographical template of immobile nanoposts and the random initial condition of density fields. The resulting self-assembled structure will be compared with the target structure (Figure 1e).

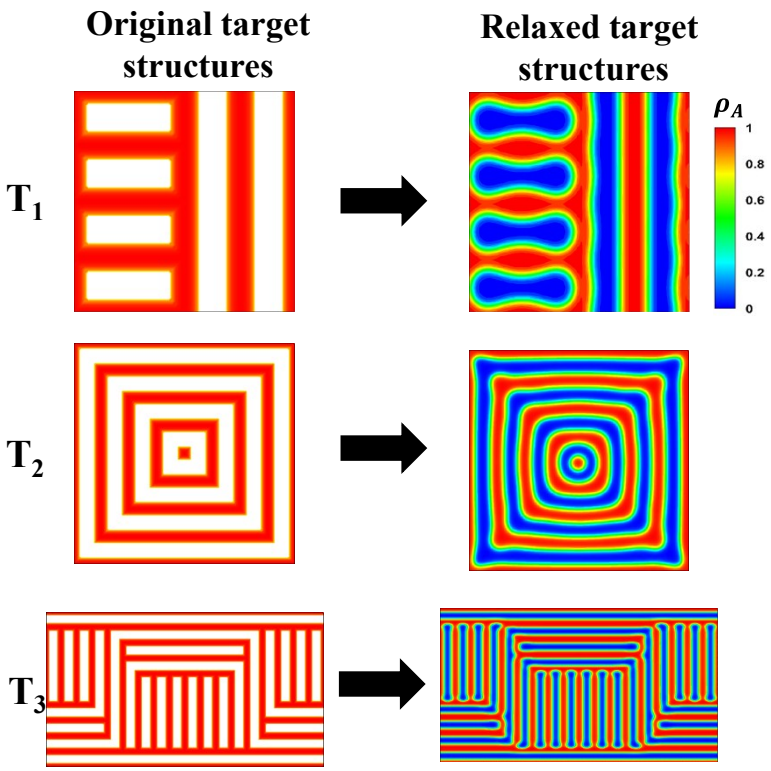

Figure S1. Simulations of symmetric AB block copolymers with the constraint of density fields for target structures. (Left panel) Constrained fields of A blocks. T_1: T-junctions and isolated line; T_2: nested-elbow structure; T_3: Large-area aperiodic structure. Red color denote the constraint of $\rho_A^T = 1.0$. (Right Panel) Relaxed density field of A blocks. Color bar represents the strength of density field ρ_A of A blocks. Note that the relaxed density field of A blocks server as the input configuration of target structures in Figure 1.

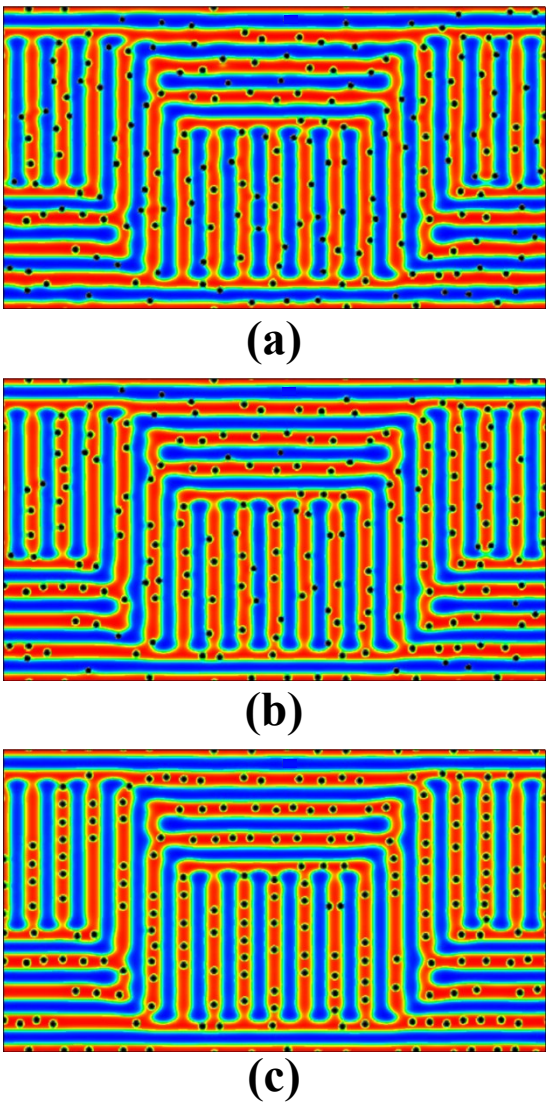

Figure S2. Typical configurations of nanoposts in the presence of constrained fields of target structure T_3. (a) #Iteration=1, (b) #iteration=500, and (c) #iteration=10000. The target structure T_3 is introduced by the Lagrange method. As the iteration step of simulations goes by, the mobile nanoposts are moved towards the A-rich domains as well as T-junctions and bends.

Part B: Fidelity Parameter

To evaluate the difference between the target and resulting structures, we calculate fidelity parameter *via* the skeletonization algorithm, where the discrete space of grid is the same as that used in the SCFT simulations. A visual outline of the calculation of fidelity parameter is depicted in Figure S3. First of all, the density fields of the target and resulting structures are thresholded to create binary images, where the value is 1 at $\rho_A(\mathbf{r})>0.5$ and 0 at $\rho_A(\mathbf{r})\leq 0.5$ for the target structure (1 at $\rho_A(\mathbf{r})+\rho_P(\mathbf{r})>0.5$ for the resulting structure). The skeletonization algorithm proposed by Zhang and Suen is applied to generate skeleton lines of domains with value of 1.[S9] As shown in Figures S3a and S3b, the skeleton lines of target and resulting structures are respectively represented by the binary map $M_T(\mathbf{r})$ and $M_R(\mathbf{r})$ defined as

$$M_{I=T,R}(r)=\begin{cases}1 & skeleton\ line\ across\ grid\ point\ r\\ 0 & else\end{cases} \quad \text{(S7)}$$

Subsequently, we introduce subtraction operator $\ominus$ to identify the differences of skeleton lines between the target and resulting structures. For instance, comparison of skeleton lines of target structures at the grid point **r** with these of resulting structures at the nearest grid point **r'** is given by

$$P_{RT}(r)\equiv M_R(r')\ominus M_T(r)=\begin{cases}1 & min\left(\left|r'-r\right|\right)>r_{cut}\ and\ M_R(r')=M_T(r)=1\\ 0 & else\end{cases} \quad \text{(S8)}$$

where the cutoff distance r_{cut} is set as $2\Delta x$ (Δx: discrete space of grid) to tolerate a slight deviation from the target structures. Given such definition, $P_{RT}(\mathbf{r})=0$ implies that the skeleton lines of resulting structures at grid point **r** match these of target structure (green squares in Figure S3c), while $P_{RT}(\mathbf{r})=1$ suggest the incorrect match (red squares). Similarly, we introduce the subtraction operator $P_{TR}(r)\equiv M_T(r')\ominus M_R(r)$ to compare the skeleton lines of resulting structures at the grid point **r** with these of target structures at the nearest grid

point **r'**. $P_{TR}(\mathbf{r})$=0 suggests the match between the target and resulting structures at grid point **r** (green squares in Figure S3d), but $P_{TR}(\mathbf{r})$=1 suggests the missing case of resulting structures in comparison to the target structures (red squares).

Finally, addition operator is defined as

$$\Omega(r) \equiv P_{RT}(r) \oplus P_{TR}(r) = \begin{cases} 1 & incorrect\ or\ missing\ match \\ 0 & well\ match \end{cases} \quad \text{(S9)}$$

The incorrect or missing matches between the target and resulting structures are represented by the red squares in Figure S3e. The fidelity parameter ξ is given by

$$\xi = \frac{N_{M_T(r)=1} - N_{\Omega(r)=1}}{N_{M_T(r)=1}} \quad \text{(S10)}$$

where $N_{M_T(r)=1}$ represents the total point number of skeleton lines of target structures and $N_{\Omega(\mathbf{r})=1}$ corresponds to the number of incorrect/missing points of resulting structures. As the fidelity parameter ξ is large, the matching degree between the target and resulting structures becomes well. As the fidelity parameter is larger than the critical value ξ_c=0.98, the inverse solutions of topographical templates have the capability to reproduce the target structures. It should be pointed out that the fidelity parameter ξ could be negative if the topographical templates are inefficient.

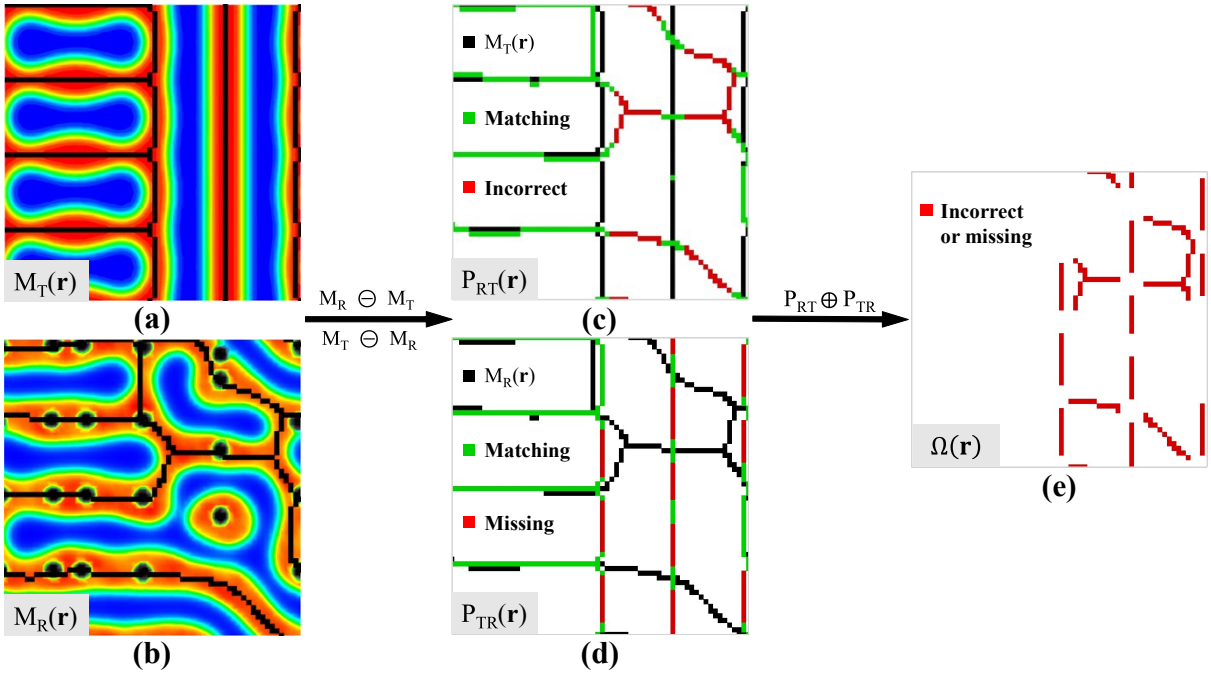

Figure S3. Visual outline of calculation of fidelity parameter. (a) Skeletonization of A-rich domains of target structure. (b) Skeletonization of A-rich and nanoparticle domains of resulting structure. In images (a) and (b), skeletonized lines M_T and M_R highlighted by black lines are overlaid on the original density field of A blocks. (c) Binary image of $P_{RT}(r) \equiv M_R \ominus M_T$. The subtraction operator $\ominus$ refers to the text. (d) Binary image of $P_{TR}(r) \equiv M_T \ominus M_R$. In images (c) and (d), the green squares denote the well match between the target and resulting structures at given points. The red squares denote the incorrect or missing case. The skeletonized lines are represented by the black squares (Note that the green squares are overlaid on the black squares under the condition of exact match). (e) Binary image of addition operator $\Omega(r) \equiv P_{RT} \oplus P_{TR}$. The red squares highlight the incorrect or missing match.

Part C: Additional Figures

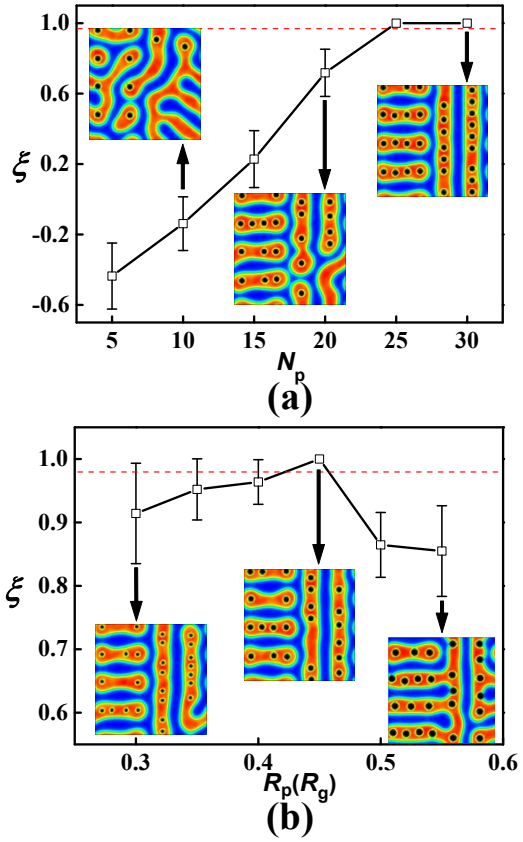

Figure S4. (a) Fidelity parameter ξ as a function of the number N_p of nanoposts for the target structure T_1. The radius of nanoposts is fixed at R_p=0.45R_g. (b) Fidelity parameter ξ as a function of the radius R_p of nanoposts. The number of nanoposts is fixed at N_p=25. Insets are the resulting structures directed by the inverse solutions of topographical templates. The dashed line represents the critical value ξ_c of fidelity parameter. Note that the target structures are translated by 2.0R_g along both *x*- and *y*- axes. The nanoposts are attractive to the B blocks.

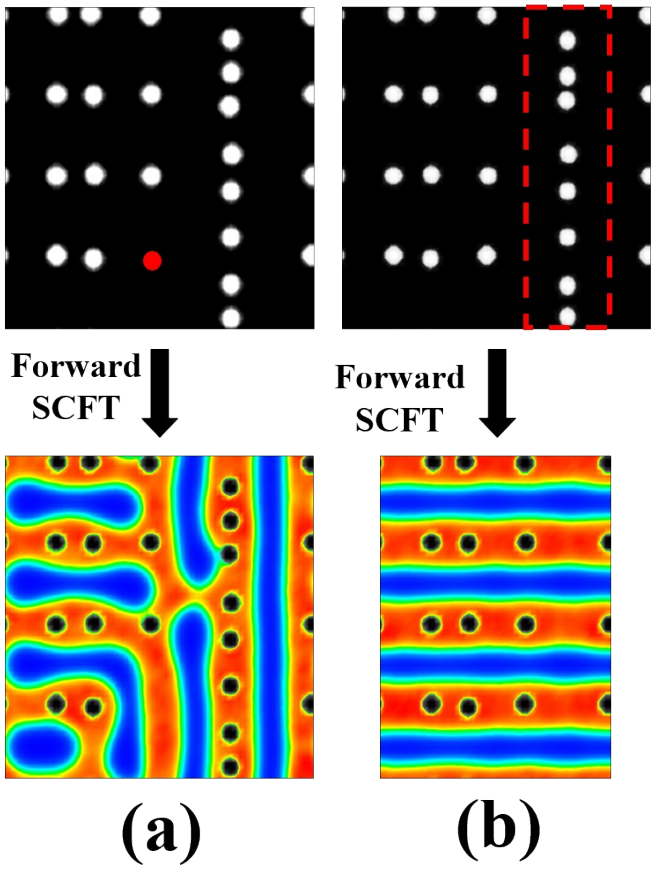

Figure S5. (a) Self-assembled nanostructure of block copolymers directed by the topographical template *via* removing one red nanopost. (b) Final nanostructure registered by the topographical template *via* removing an array of nanoposts enclosed by red rectangle. The original topographical template is shown in Figure 3a of main text.

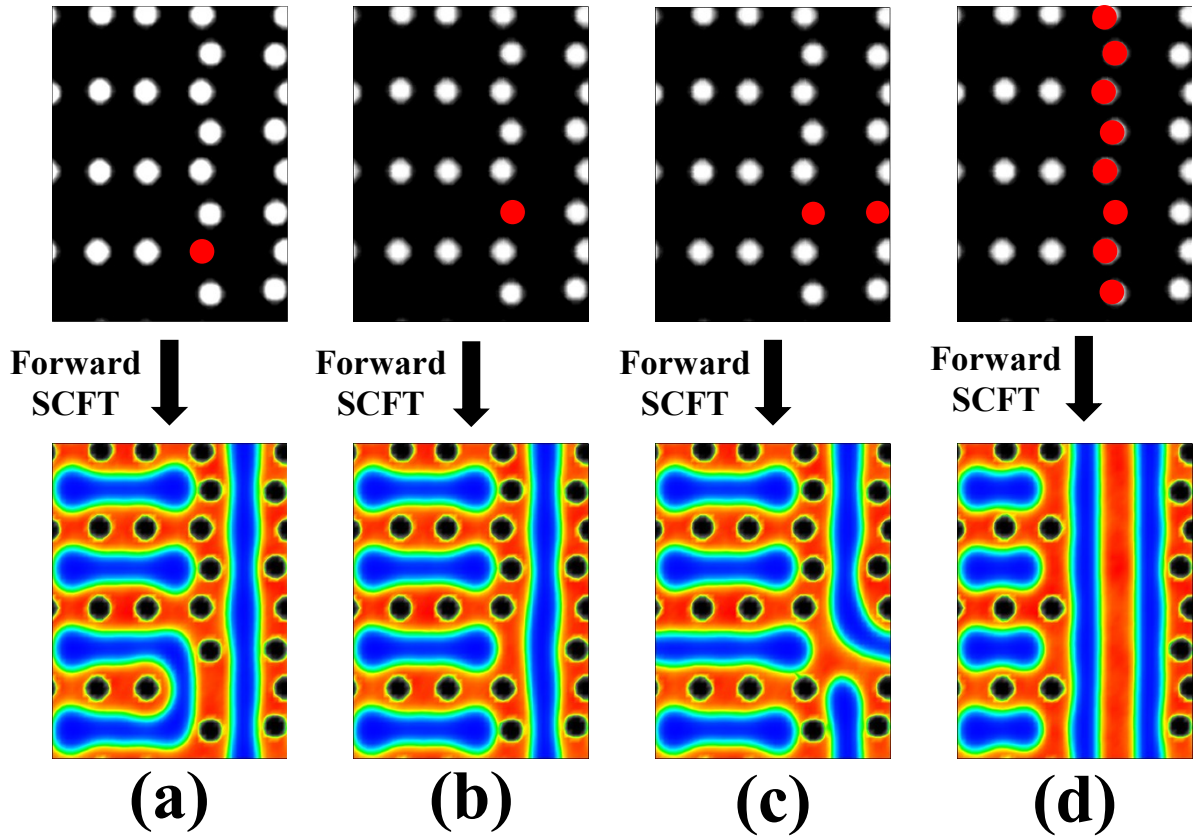

Figure S6. Self-assembled nanostructures of block copolymers directed by the topographical templates *via* removing nanoposts highlighted by red color. (a) Removing nanopost at the center of T-junction, (b) removing nanopost at the interspace of adjoining T-junctions, (c) removing a pair of nanoposts at the interspaces, and (d) removing an array of nanoposts. The original topographical template is shown in Figure 5d of main text.

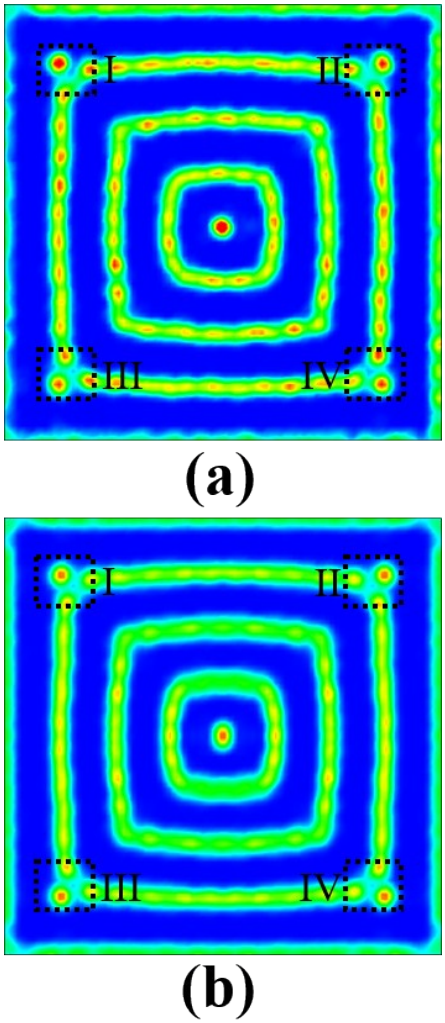

Figure S7. (a) Probability distribution of nanoposts. (b) Probability distribution of nanoposts after symmetric operation. The symmetric operation of probability distribution P at grid point (i, j) is defined as $P_{i,j}=(P_{i,j} + P_{Nx-i,j} + P_{i,Ny-j} + P_{Nx-i,Ny-j})/4$, where N_x and N_y are respectively the grid number of simulations along the x and y directions. The Roman numbers match the labels in Figure 6b of main text.

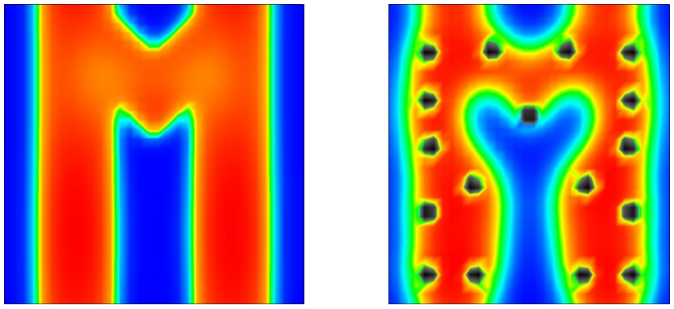

Figure S8. (a) M-like target structure with size of $8R_g \times 8R_g$. (b) Inverse solution of topographical template and corresponding self-assembled nanostructure of block copolymers. The input parameters of inverse design algorithm are chosen as N_p=16 and R_p=0.25R_g. With the help of deduced template, the block copolymers self-assemble into the M-like nanostructure. Through the skeletonization analysis, it is further confirmed that the resulting nanostructure matches well with the target one (*i.e.*, the fidelity parameter ξ = 1.0).

References

S1 S. W. Sides, B. J. Kim, E. J. Kramer and G. H. Fredrickson, *Phys. Rev. Lett.*, 2006, **96**, 250601.

S2 Q. Zhang, L. Zhang and J. Lin, *J. Phys. Chem. C*, 2017, **121**, 23705−23715.

S3 K. S. Lyakhova, A. V. Zvelindovsky, G. J. A. Sevink and J. G. E. M. Fraaije, *J. Chem. Phys.*, 2003, **118**, 8456.

S4 G. H. Fredrickson, *The Equilibrium Theory of Inhomogeneous Polymers*, Oxford University Press: New York, 2006.

S5 L. Zhang, J. Lin and S. Lin, *Macromolecules*, 2007, **40**, 5582–5592.

S6 L. Zhang, J. Lin and L. Wang, *ACS Macro Lett.*, 2014, **3**, 712–716.

S7 Q. Zhang, L. Zhang and J. Lin, *Nanoscale* 2019, **11**, 474–484.

S8 R. B. Thompson, V. V. Ginzburg, M. W. Matsen and A. C. Balazs, *Science*, 2001, **292**, 2469–2472

S9 Y. Kim, H. Chen and A. Alexander-Katz, *Soft Matter*, 2014, **10**, 3284−3291.

S10 J. Koski, B. Hagberg and R. A. Riggleman, *Macromol. Chem. Phys.*, 2016, **217**, 509-518.

S11 T. Y. Zhang and C. Y. Suen, *Commun. ACM*, 1984, **27**, 236−239.